sustainability

MDPI

Article

Modified Nanocellulose-Based Adsorbent from Sago Waste for Diclofenac Removal

Noorhaslin Che Su [1], Ain Aqilah Basirun [1], Nor Shahroon Hameed Sultan [1], Devagi Kanakaraju [2] and Cecilia Devi Wilfred [1,3,*]

[1] Centre of Research in Ionic Liquid, Universiti Teknology PETRONAS, Persiaran UTP, Seri Iskandar 32610, Perak, Malaysia
[2] Faculty of Resource Science and Technology, Universiti Malaysia Sarawak, Kota Samarahan 94300, Sarawak, Malaysia
[3] Fundamental and Applied Sciences Department, Universiti Teknologi PETRONAS, Persiaran UTP, Seri Iskandar 32610, Perak, Malaysia
* Correspondence: cecili@utp.edu.my

Abstract: A nanocellulose-based adsorbent was successfully synthesized via a hydrothermal process. It was characterized by X-ray diffraction, Fourier Transform Infrared Spectroscopy, Field Emission Electron Microscopy and Brunauer–Emmett–Teller surface area analysis. Photocatalysis has the best potential to replace the conventional wastewater treatment technology through the photodegradation of organic contaminants. This study focuses on the preparation of a photocatalytic adsorbent of nanocellulose prepared from sago waste for the removal of diclofenac from industrial wastewater. Its photocatalytic activity was evaluated through the degradation of diclofenac (100 mg/L) under ultraviolet (UV) light. The effect of different loadings of TiO_2 and kinetics on the photocatalytic activity was investigated. To study its removal, the experiments were carried out under UV light with different contact times ranging from 30 to 120 min at room temperature. The maximum removal percentage was found to be 57.5% for 200 µL of TiO_2, and this increased up to 82.4% for 800 µL of TiO_2. The maximum removal capacity was found to be 13.3 mg/g. The kinetics was well fitted with "pseudo-first order model" (PSO). Kinetic analysis using the PSO model at 100 ppm of diclofenac sodium gave a value of equilibrium adsorption capacity, qe of 13.52 mg/g. The adsorption kinetics gave a value of calculated equilibrium adsorption capacity, qe of 13.52 mg/g using different non-linear regression plots. It obeyed a pseudo-first-order reaction with the lowest AICc, RSME values of 0.56 and 0.53 and the highest correlation coefficient, R^2, of 0.99. Three kinetics models were fitted for the current adsorption kinetics data, and their suitability was inferred as the following: pseudo-first-order > pseudo-second-order > Langmuir–Hinshelwood.

Keywords: nanocellulose; magnetite; titanium dioxide; photocatalyst; kinetic study; diclofenac

Citation: Che Su, N.; Basirun, A.A.; Hameed Sultan, N.S.; Kanakaraju, D.; Wilfred, C.D. Modified Nanocellulose-Based Adsorbent from Sago Waste for Diclofenac Removal. *Sustainability* **2023**, *15*, 5650. https://doi.org/10.3390/su15075650

Academic Editor: Antonio Zuorro

Received: 2 February 2023
Revised: 14 March 2023
Accepted: 15 March 2023
Published: 23 March 2023

1. Introduction

Diclofenac (DCF) is widely used to treat fever, pain, rheumatoid arthritis, etc. [1–3]. The molecule is readily absorbed from the gastrointestinal tract. However, is water insoluble. DCF has been detected in µg/L in in drinking water, ground water and surface water all around the world. It can cause harmful effects on both human health and aquatic ecosystems, such as cytopathological symptoms in the gills, kidneys and liver of rainbow trout. DCF cannot be removed effectively by conventional wastewater treatment due to its stable chemical structure. Therefore, it is essential to develop more effective and sustainable treatment technologies for the removal of DCF and to treat and reuse wastewater.

Over the years, there has been increasing research into the application of nanocellulose (NC) as a smart material for water purification. Several studies have proven that NC provide greater surface areas, functional groups, water insolubility and high holding ability

to extract heavy metal ions in wastewater treatment [4,5]. In addition, they offer effective and affordable treatment strategies at minimal cost.

Advanced oxidation processes (AOPs) including electrochemical oxidations, photocatalysis, photo-Fenton and ultraviolet/H_2O_2 have been employed to remove contaminants from wastewater. In recent years, photocatalyst technology has been a hot research area [3,6–8]. Heterogeneous photocatalysis is an advanced oxidation process based on light and semiconductors to generate oxidizing/reducing species dealing with environmental pollutants. Non-toxic, chemically stable titanium dioxide (TiO_2) is the most widely studied as a photocatalyst [9–11]. Adequate photon energy (*hv*) irradiated onto TiO_2 particle surfaces (3.2 eV (anatase form) or 3.0 eV (rutile form)) will create electron–hole pair formation (e^-–h^+). The photonic excitation leaves behind an empty unfilled valance band, thus creating the electron–hole pair. The series of chain oxidative–reductive reactions that occur at the photon-activated surfaces is postulated as below [12]:

$$\text{Photoexcitation: } TiO_2 + hv \rightarrow e^+ + h^+ \quad (1)$$

$$\text{Charge} - \text{carrier trapping of } e^-\text{: } e^-_{CB} \rightarrow e^-_{TR} \quad (2)$$

$$\text{Charge} - \text{carrier trapping of } h^+\text{: } h^+_{VB} \rightarrow h^+_{TR} \quad (3)$$

$$\text{Electron} - \text{ hole recombination: } e^-_{TR} + h^+_{VB}\ (h^+_{TR}) \rightarrow e^-_{CB} + \text{heat} \quad (4)$$

$$\text{Photoexcited } e^- \text{ scavenging: } (O_2)_{ads} + e^- \rightarrow O_2^{\bullet -} \quad (5)$$

$$\text{Oxidation of hydroxyls: } OH^- + h^+ \rightarrow OH\cdot \quad (6)$$

$$\text{Photodegradation by OH : } R - H + OH\cdot \rightarrow R'\cdot + H_2O \quad (7)$$

The e^-_{TR} and h^+_{TR} in (Equation (4)) represent the surface-trapped valence-band electron and conduction-band hole, respectively. It was reported that these trapped carriers are usually TiO_2-surface-bound and do not recombine immediately after photon excitation. In the absence of electron scavengers (Equation (4)), the photoexcited electron recombines with the valence band hole in nanoseconds with the simultaneous dissipation of heat energy. Thus, the presence of electron scavengers is vital to prolong the recombination and successful functioning of photocatalysis. Equation (5) depicts how the presence of oxygen prevents the recombination of electron–hole pairs, while allowing the formation of superoxide radical $O_2^{\bullet -}$.

NC can be applied for various approaches and possibly functions such as filters, adsorbents or membranes depending on the structure of the pore and the method of preparations. In this study, an adsorbent based on photocatalysis was prepared. The interaction of magnetite (Fe_3O_4) has attracted much attention with TiO_2 as it influences photocatalytic activity due to its large surface area to volume ratio which offer high capacity for adsorption in wastewater treatment [13]. Thus, mixing TiO_2 with magnetite and nanocellulose may provide a more sustainable use in water treatment involving adsorption [14,15] and photocatalytic activity [16].

Herein, we were able to develop a novel NC/Fe_3O_4/TiO_2 adsorbent via a hydrothermal process. Mathematical models were used quantitatively to predict and correlate adsorption capacities/strengths and to design adsorptive processes. Modelling facilitates our understanding of biosorption dynamics, the anticipation of responses, improvements in biosorption processes, and the analysis of data [17]. Kinetics and isotherms are important in moving technology from the laboratory to the industrial scale. Kinetics describes the rate of the adsorption process, whereas isotherms represent the equilibrium connection between sorbent and adsorbent concentrations at a fixed temperature. The Akaike Information Criterion (AICc), the Root Mean-Square Error (RMSE), and the adjusted Determination Coefficient (R^2) were used to determine the best-fit kinetic reaction of the present study [17].

2. Materials and Methods

2.1. Materials

Nanocellulose was prepared from sago bark waste collected from a sago industry in Sarawak. Iron (III) hexahydrate ($FeCl_3 \cdot 6H_2O$), iron (II) chloride tetrahydrate ($FeCl_2 \cdot 4H_2O$), trisodium citrate ($Na_3C_6H_5O_7$), sodium hydroxide (NaOH), titanium (IV) n- butoxide (TBOT) and ethanol were purchased from Merck. Sodium hydroxide (NaOH) and sodium acetate were purchased from Sigma Aldrich. Diclofenac (Brand: Dicloran-USP; 50 mg; pharmaceutical grade) was obtained from a local pharmacy.

2.2. Preparation of Nanocellulose Adsorbent

The methods for the preparation of the nanocellulose adsorbent are described below.

2.2.1. Isolation of Cellulose

Alkaline treatment was used to eliminate the amorphous polymer of hemicellulose and the remaining lignin [18]. The bleaching process was carried out using hydrogen peroxide. The white color of the fiber of cellulose obtained after the bleaching process indicated the successful removal of lignin and other impurities.

2.2.2. Preparation of Nanocellulose

To produce nanocellulose, 1 g of extracted cellulose was hydrolyzed with H_2SO_4 (40 wt.%) at 45 °C for 60 min in a ratio of 1:20. After hydrolysis, the suspension was washed repeatedly with cold deionized water. It was later centrifuged at 4000 rpm for 30 min, which gave a pearl white sediment. The slurry was further sonicated for 40 min and dried [5]. The nanocellulose powder was characterized by X-ray diffraction (XRD).

2.2.3. Synthesis of Magnetite (Fe_3O_4)

The Fe_3O_4 nanoparticles were synthesized using the chemical coprecipitation method. Fe^{3+} and Fe^{2+} with a molar ratio of 1: 2 in the form of iron (II) chloride tetrahydrate (1.00 g, 0.005 mol) and iron (III) chloride hexahydrate (2.70 g, 0.010 mol) were dissolved in 130 mL of distilled water with vigorous stirring for 2 h. Then, 30 mL of NaOH (2M) was added rapidly into the mixture, which formed a black precipitate, Fe_3O_4. The mixture was then heated to 60 °C for 1 h. The mixture was left to cool down to room temperature, and the magnetite was washed several times with distilled water and ethanol until a pH value of 7 was achieved. The magnetite was redispersed for 30 min in 200 mL of trisodium citrate solution (0.3 M) before being heated at 80 °C for 1 h. This was to cap the particles from further growth. The magnetite was then collected and washed with acetone to remove any remnant of trisodium citrate. Finally, the magnetite was redispersed in 100 mL of distilled water for 30 min to form a stable ferrofluid. The prepared ferrofluid was stored in a fridge (4 °C) until further use [16].

2.2.4. Synthesis of Nanocellulose/Magnetite Adsorbents (Fe_3O_4)

The magnetic nanocellulose/magnetite was synthesized using the hydrothermal method. First, 0.5 g of nanocellulose was dissolved in 20 mL of H_2O with vigorous mechanical stirring at 80 °C in a water bath until a homogeneous viscous solution was formed. Subsequently, 0.45 g of Fe_3O_4 and 1.21 g of sodium acetate were added to the nanocellulose solution with vigorous agitation for 30 min at 80 °C in a water bath to form a homogeneous solution. The solution was poured into a Teflon-lined stainless-steel autoclave for hydrothermal treatment at 110, 130 and 150 °C for 4 h. It was later cooled to ambient temperature; the black precipitate product was separated by a magnet and washed several times with water and ethanol. The as-prepared samples were dried overnight at 50 °C in an oven [19].

2.2.5. Synthesis of Nanocellulose/Fe_3O_4/TiO_2

A total of 0.10 g of nanocellulose/Fe_3O_4 powder was added into a 10 mL absolute ethanol solution and sonicated for ca. 20 min in an ultrasonic bath to obtain a homogenous colloidal solution. An amount of 200 µL of TBOT was added into the dispersion dropwise, and the mixture was sonicated for 15 min. It was then decanted into a vapor-phase hydrolysis apparatus (VPHA) with deionized water situated at the bottom of it to produce vapor at a raised temperature. The closed VPHA was heated to 110 °C and maintained for 5 h. Then, the VPHA was cooled to room temperature. The as-prepared powder was collected by a magnet and washed with absolute ethanol and deionized water and dried in the oven at 50 °C. The same procedure was repeated to prepare the adsorbent with various concentrations of TiO_2. Table 1 describes the various types of adsorbent prepared [16,19].

Table 1. Synthesized adsorbent with various dosages of TiO_2.

Adsorbent	Sample Code
Nanocellulose/Fe_3O_4	NC/Fe_3O_4
Nanocellulose/Fe_3O_4/TiO_2 (200 µL)	Ads-1
Nanocellulose/Fe_3O_4/TiO_2 (400 µL)	Ads-2
Nanocellulose/Fe_3O_4/TiO_2 (800 µL)	Ads-3

2.3. Photocatalytic Reaction

Ultraviolet (UV) light photocatalytic reactions were carried out to characterize the degradations rate of diclofenac. The suspension was irradiated with an ultraviolet lamp. First, 0.1 g/L adsorbent was added to wastewater. Prior to the photocatalytic process, wastewater containing adsorbent was stirred and stored in the dark for 30 min. The diclofenac concentration was determined in the sequence of 30, 60, 90 and 120 min using a Lamba 35 UV light (Perkiin Elmer, Walthham, MA, USA). The photocatalytic activity of the adsorbent was evaluated in terms of the degradation of diclofenac in wastewater under UV-light illumination. The initial concentration of diclofenac was 100 mg/L. The suspension was stirred magnetically (200 rpm) in the dark for 30 min to reach the absorption/desorption equilibrium of the adsorbent as well as to obtain the maximum absorption of diclofenac. At the end of the first 30 min, a sample of 10 mL was taken from the wastewater by means of syringe filters (Millex Millipore, Carrigtwohill, Ireland: 0.22 µm). After the first measurement, the UV lamp was turned on, and changes in absorption under UV light were measured. A 100 W UV lamp (UVP Co., Upland, CA, USA) was used for the UV light source at the wavelength of 365 nm. The same procedure was applied after 30, 60, 90 and 120 min of UV light illumination. It is assumed that holes (h^+) reacted with water molecules (H_2O), which were adsorbed on the TiO_2 surface, to generate hydroxyl radicals ($OH^{\cdot}$), which assisted in the degradation of the diclofenac (Figure 1).

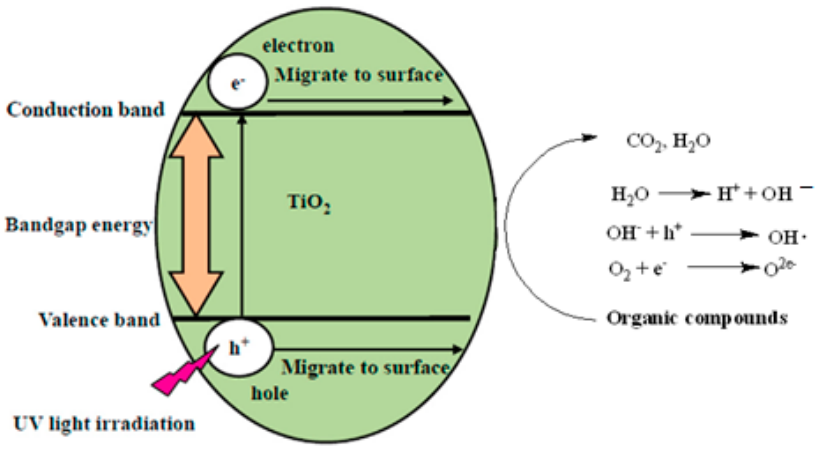

Figure 1. The schematic diagram of the photocatalytic degradation of the organic compound [9].

The mechanism of diclofenac removal via photocatalysis were discussed by Martínez and team [20]. The diclofenac removal was calculated by the following Equation (8):

$$R\ (\%) = [C_0 - C_1)/C_0] \times 100 \quad (8)$$

where R is diclofenac removal percent, C_0 is the initial diclofenac concentration in ppm and C_1 is the concentration of diclofenac solution after irradiation in ppm.

2.4. Characterization

The nanocellulose powders' phase compositions were identified by X-ray diffraction (XRD) equipment (D/max 2550 PC, Rigaku Co., Tokyo, Japan) using Cu K_α radiation at 40 Kv and 200 mA. The morphology was studied using a field emission scanning electron microscope (FESEM) (Model: Zeiss, Supra 55VP, Jena, Germany) equipped with an energy-dispersive X-ray and field emission scanning electron microscope (Model: Clara Tescan, Brno, Republic Czech). The samples were coated using a gold coater. The nitrogen adsorption and desorption isotherms were obtained at 77K using Autosorb -1 MP (Quantachrome, Boynton Beach, FL, USA) utilizing Barrett–Emmett–Teller calculations of pore volume and pore size (diameter) distributions from the desorption branch of the isotherm. The FTIR spectra of the samples were recorded using the PerkinElmer Spectrum in the range of 4000 cm^{-1} to 500 cm^{-1} at 4 cm^{-1} resolution using PerkinElmer Fourier-Transform infrared attenuated total reflection (FTIR-ATR).

2.5. Kinetic Study

The concentration of the solution of the absorbent–absorbate solution at various time intervals was determined [21–23]. The quantity absorbed at time t, denoted by the symbol q_t (mg/g), was estimated using Equation (9). q_t denotes the removal capacity by 1 g of absorbent at a certain time of exposure. It was assessed by performing an adsorption study under optimal conditions at certain time intervals until the adsorption reached an equilibrium, in this case 120 min. The non-linear regression of all kinetic models was plotted and analyzed using Curve Expert 6.0. The removal rate was assumed to be proportional to the difference between the extracted concentration and the number of accessible sites in the pseudo-first-order equation (PFO) proposed by Lagergren for solid–liquid systems [22]. The pseudo-first-order kinetic model equation is as follows:

$$q_t = q_e\left(1 - e^{-k_1 t}\right) \quad (9)$$

A second-order relation between the adsorption rate and the difference between saturation concentrations is proposed in the pseudo-second-order model (PSO), which implies that chemisorption is the rate-limiting step. The equation for the pseudo-second-order kinetic model is shown in Equation (10). The model is based on the adsorption capacity onto a solid phase, and the nonlinear form of PSO was initially proposed by Blanchard et al. It is expressed as:

$$q_t = \frac{k_t q e^2 t}{1 + k_2\, q_e t} \quad (10)$$

Langmuir–Hinshelwood (LH) kinetics is the most commonly used kinetic expression to explain the kinetics of catalytic processes [24]. The Langmuir–Hinshelwood expression that explains the kinetics of catalytic systems is given by:

$$qt = -\frac{dC}{dt} = \frac{k_t K C}{1 + KC} \quad (11)$$

where q_t represents the rate of reaction that changes with time.

The model involves two steps: the adsorption of reactants onto the catalyst surface and reaction of the adsorbed species. The rate of the overall reaction is determined by the rate of the slower step.

The term r in Equation (11) was represented in terms of the initial reaction rate, r_0, as a function of the initial diclofenac concentration, C_0, or in terms of C_e, where C_e is the equilibrium diclofenac concentration in solution after the completion of dark experiments. The initial rate of the reaction as a function of C_0 and C_e is given by Equations (12) and (13), respectively:

$$qt = \frac{k_t K C_0}{1 + K C_0} \tag{12}$$

$$qt = \frac{k_t K C_e}{1 + K C_e} \tag{13}$$

2.6. Statistical Analysis

For all models tested in this study, statistical discriminatory tests such as Root-Mean-Square Error (RMSE), corrected AICc (Akaike Information Criterion), accuracy factor (AF) and bias factor (BF) and adjusted coefficient of determination (R^2) were utilized in this work. All the parameter estimations were made using CurveExpert 6.0.

The RMSE was calculated according to Equation (14) where n is experimental data points, Ob_i and Pd_i are the experimental and predicted data, respectively, while p is parameter numbers [17].

$$RMSE = \sqrt{\frac{\sum_{i=1}^{n} (Pd_i - Ob_i)^2}{n - p}} \tag{14}$$

The Akaike Information Criterion (AIC) *AICc*, which is based on the information theory [23], is calculated as follows (Equation (15)):

$$AICc = 2p + n \ln\left(\frac{RSS}{n}\right) + 2(p+1) + \frac{2(p+1)(p+2)}{n - p - 2} \tag{15}$$

Further error function analyses are the Accuracy Factor (AF) and Bias Factor (BF) (Equations (16) and (17)).

$$\text{Bias factor} = 10^{\left(\sum_{i=1}^{n} \log \frac{(Pd_i/Ob_i)}{n}\right)} \tag{16}$$

$$\text{Accuracy factor} = 10^{\left(\sum_{i=1}^{n} \log \frac{|(Pd_i/Ob_i)|}{n}\right)} \tag{17}$$

3. Results and Discussions

Figure 2 shows the XRD peak for raw sago and nanocellulose. The crystallinity index, *CrI* for each sample, was determined based on Equation (18) [25]:

$$CrI = \frac{I_{002} - I_{am}}{I_{am}} \tag{18}$$

where I_{002} is the maximum intensity of the (0 0 2) lattice diffraction peak and I_{am} is the intensity scattered by the amorphous part of the sample. The diffraction peak for plane (0 0 2) is located at a diffraction angle around 2θ = 22°, and the intensity scattered by the amorphous part is measured as the lowest intensity at a diffraction angle around 2θ = 18°. The crystallinity index for raw sago and nanocellulose is 23% and 73%, respectively. The crystallinity of nanocellulose demonstrates higher crystallinity because of the efficient removal of the amorphous parts by the cleavage of glycosidic linkages releasing crystallites [8].

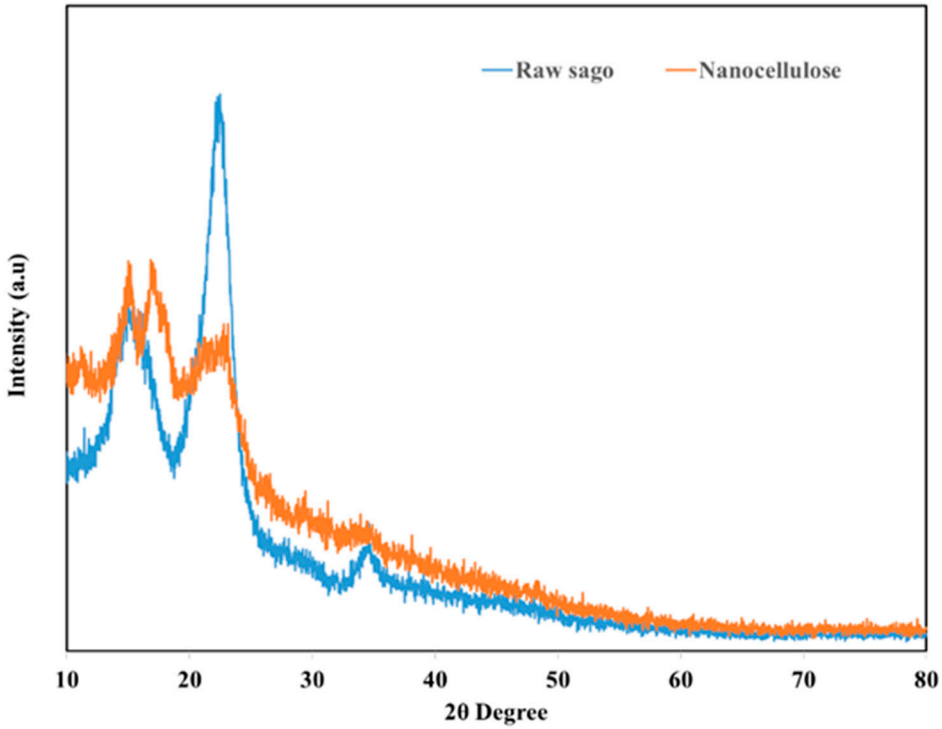

Figure 2. XRD peak for raw sago and nanocellulose.

Figure 3 shows the XRD peak for nanocellulose/Fe_3O_4 prepared at different temperatures. The peaks at 2θ = 30.1°,35.3°, 43° and 53.3° and 62.7° stand for [(220), (311), (400), (422) and (440)] which are consistent with the main phases of the magnetite (Fe_3O_4)—JCPDS card no. 019–0629 [19]. The peaks at 2θ = 18.2°, 30.5°, 35.7°, 43.4°, 53.55°, 57.5° and 62.9° stand for the (111), (220), (311), (400), (422), (511) and (440) planes, representing the nanocellulose/Fe_3O_4. These peaks appeared to have weak intensities due to the interaction of magnetite and nanocellulose [26]. The nanocellulose/Fe_3O_4 prepared at 130 °C was further added with TiO_2.

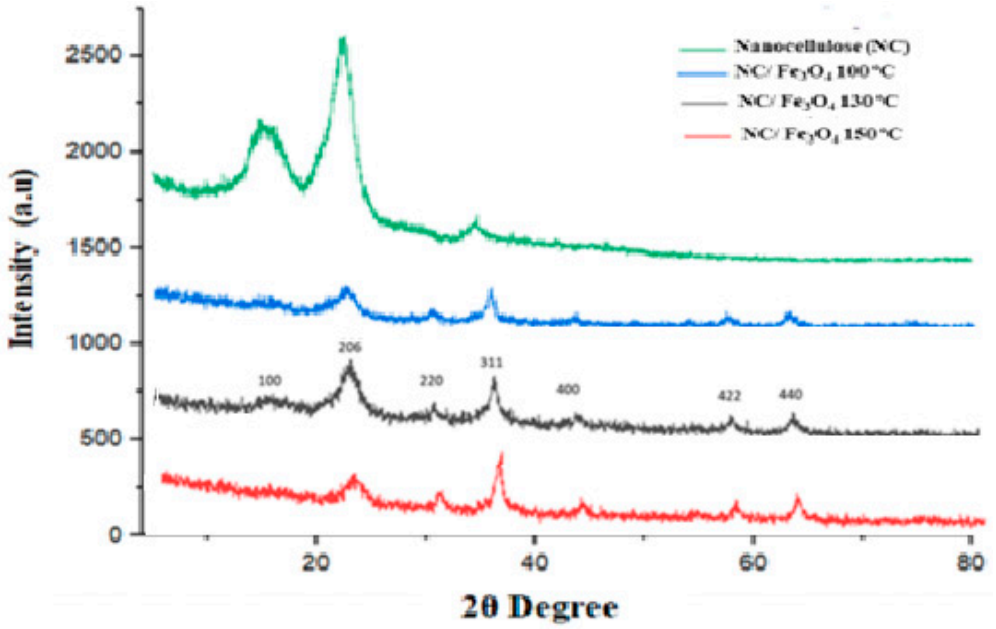

Figure 3. XRD peak for Fe_3O_4/Nanocellulose prepared at different temperatures.

Figure 4 shows the XRD peaks for nanocellulose/Fe_3O_4 and nanocellulose/Fe_3O_4/TiO_2 magnetite adsorbent. The peaks at 2θ = 30.1°, 35.3°, 43°, 53.3° and 62.7° which stand for [(220), (311), (400), (422) and (440)] are consistent with the main phases of the magnetite (Fe_3O_4)—JCPDS card no. 019-0629 [19]. The peaks at 2θ = 25.68°, 38.47°, 48.13° and 54.55° which stand for the (101), (103), (200) and (105) refer to anatase phase of TiO_2 and demonstrate the formation of well-crystallized TiO_2 (JCPDS card no 01-0562) [27]. The XRD results demonstrate that the crystalline and anatase Fe_3O_4 and TiO_2, respectively, coexisted in the adsorbent sample.

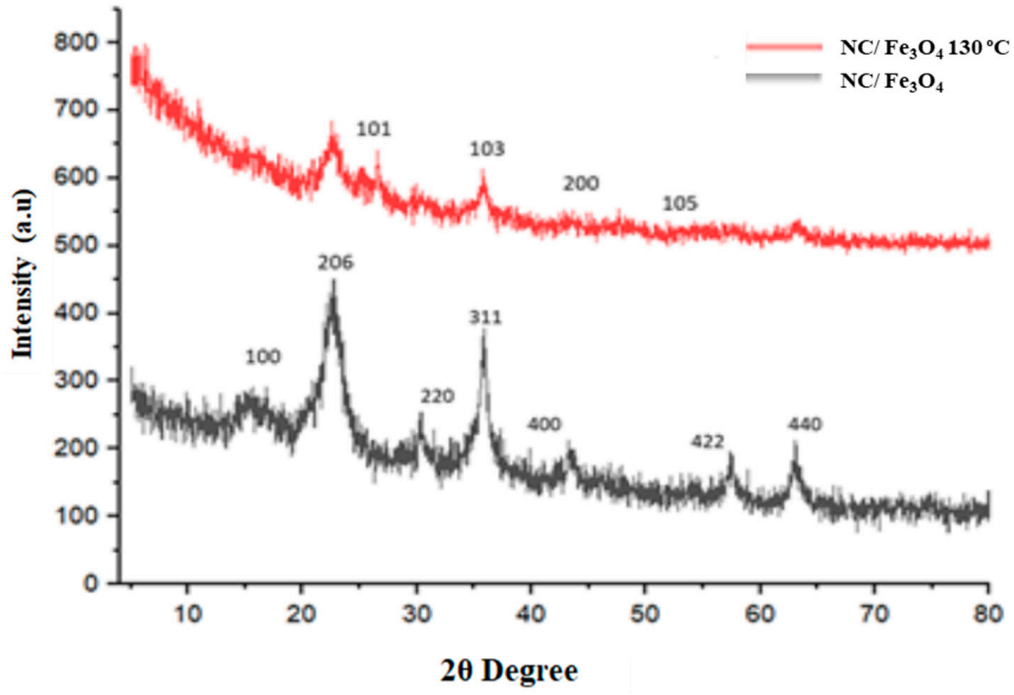

Figure 4. XRD peaks for nanocellulose/Fe_3O_4 and nanocellulose/Fe_3O_4/TiO_2.

Figure 5 shows the comparison of the FTIR spectra range of the prepared nanocellulose, Fe_3O_4, NC/Fe_3O_4, Ads-1, Ads-2 and Ads-3. The spectrum shows the appearance peaks at 1064, 1639 and 2893 cm^{-1} which represent -C-O-, C=O and -C-H stretching, respectively [28]. Meanwhile, the Fe_3O_4 spectrum shows peaks at 542 and 1647 cm^{-1} which represent Fe-O stretching and C=O, respectively [29]. Ads-1 shows the presence of nanocellulose and magnetite Fe_3O_4 peaks. A similar pattern was observed for Ads-2 and Ads-3. The wide absorption band around 3600–3000 cm^{-1} that appeared in all samples was attributed to the stretching vibration of −OH from the hydroxyl group originated from the free water molecules on the adsorbent surfaces [28,30].

Further analysis was carried out using FESEM to compare the surface morphologies of the synthesized adsorbent. Figure 5 demonstrates that NC/Fe_3O_4 appeared to have smoother appearances compared to NC/Fe_3O_4/TiO_2 (200 µL), which showed rougher surfaces. The rougher surfaces allowed more diclofenac molecules to be absorbed onto them. White particles (marked red) on the NC/Fe_3O_4/TiO_2 surface were identified as TiO_2 particles. This is supported by the EDX results. This finding shows that TiO_2 particles were well dispersed on the NC/Fe_3O_4 surface. Figure 6c shows the FESEM mapping result of Ads-1. This further confirms the presence of TiO_2 along with carbon (C) and iron (Fe).

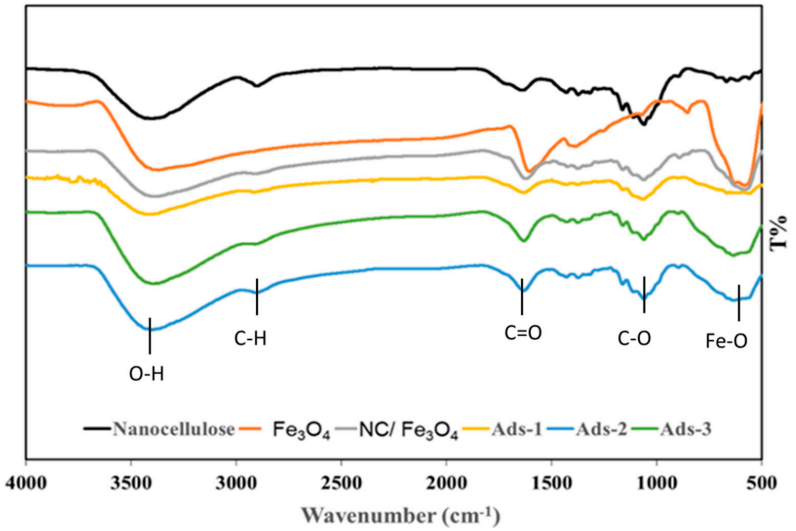

Figure 5. The FTIR spectra of nanocellulose, Fe_3O_4 (magnetite), nanocellulose + magnetite and the prepared adsorbent (Ads-1, Ads-2 and Ads-3).

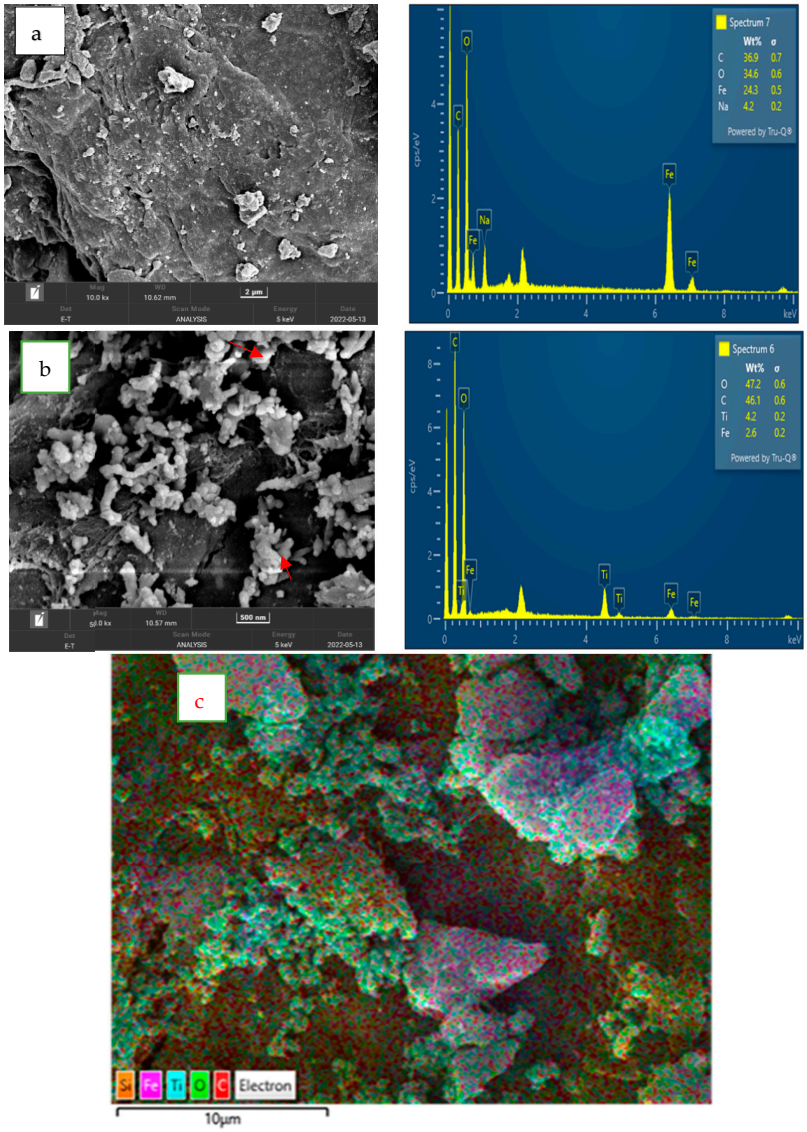

Figure 6. The FESEM of (**a**) NC/ Fe_3O_4 (**b**) Ads-1 and (**c**) mapping results of Ads-1.

The surface area, pore volume and pore diameter of prepared adsorbents were determined using BET. Based on Table 2, the prepared adsorbents could be classified in the category of mesoporous as their pore sizes were in the range of 2–10 nm. With the addition of more TiO_2 from 200 µL to 400 µL, the BET surface area increased. However, with the addition of more TiO_2 up to 800 µL, the surface area decreased, as TiO_2 tends to agglomerate and cumulate in pores [27].

Table 2. The results of BET analyses for the prepared adsorbent.

Adsorbent	BET Surface Area (m^2/g)	Pore Volume (cm^3/g)	Pore Diameter (nm)
Ads-1	74.87	0.1282	6.853
Ads-2	160.65	0.167	6.354
Ads-3	103.39	0.155	6.011

Studies on the effect of varying the adsorbent dosage of TiO_2 in NC/Fe_3O_4/TiO_2 from 200 µL to 800 µL on the DCF removal within a 120 min reaction were carried out. Upon UV irradiation, DCF removal showed 57% with 200 µL TiO_2 loading. The removal percentages displayed no significant changes (57.4%) with the addition of a TiO_2 dosage up to 400 µL. However, the removal of diclofenac increased up to 82% with the addition of an 800 µL TiO_2 dosage (Figure 7). This signifies that 800 µL pf TiO_2 is the best amount to promote maximum UV light absorption and transfer the charge carriers to the surface for photocatalytic treatment. The OH radicals that were produced in the photocatalytic process oxidized the DCF organic pollutant to intermediates/degradation products and finally to complete mineralization. The degradation pathway of DCF is reported to include hydroxylation, the cleavage of the N-H bond, dehalogenation and aromatic ring opening [10].

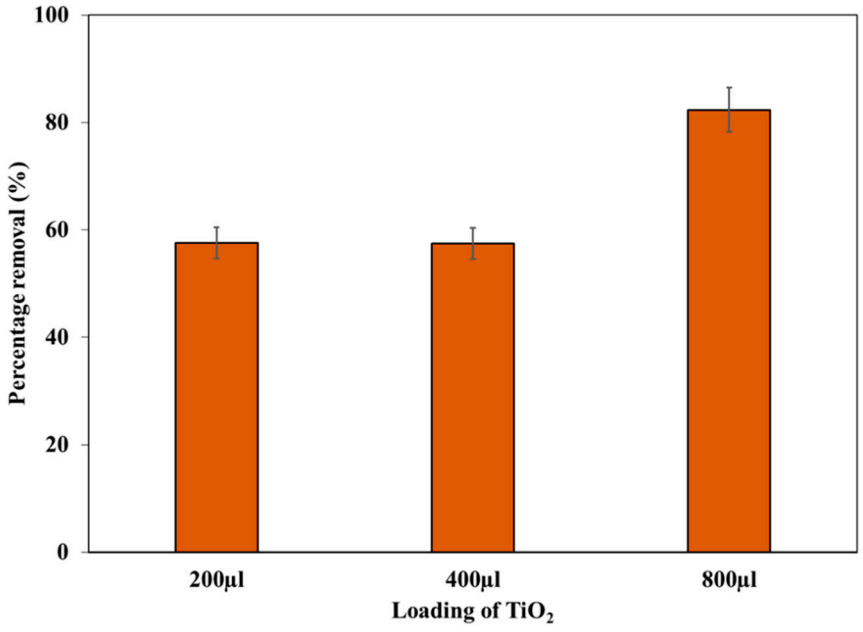

Figure 7. Percentage of diclofenac removal with different loadings of TiO_2.

Figure 8 shows the removal percentage of diclofenac as a function of time with different loadings of TiO_2. In the first 30 min in the dark, the removal of diclofenac increased up to 50% for 200 µL and 400 µL loadings of TiO_2. This shows that the presence of nanocellulose and magnetite in the adsorbent system facilitated the DCF removal through the adsorption process [16]. It is known that cellulose and magnetite are good adsorbents [31]. This shows that NC/Fe_3O_4/TiO_2 could remove 50% of DCF in dark conditions predominantly by the adsorption process. Upon UV irradiation from 30 min to 120 min, although the TiO_2

dosage increased from 200 to 400 µL, only a very small increment in DCF was removed. The removal of DCF was not greatly impacted by increasing the dosage of TiO_2 from 200 to 400 µL but was favored by the adsorption process and a minimum amount by photocatalytic activity. This finding corroborates with those reported by Kanakaraju et al. [16]. However, with a higher loading of TiO_2 at 800 µL, the removal percentage of diclofenac was seen to increase up to 87%, indicating photocatalytic activity dominates the removal of DCF. There could be more •OH radicals formed that could have aided in the removal of diclofenac. The adsorption and photocatalytic reaction behavior can be further discussed through kinetic analysis prediction.

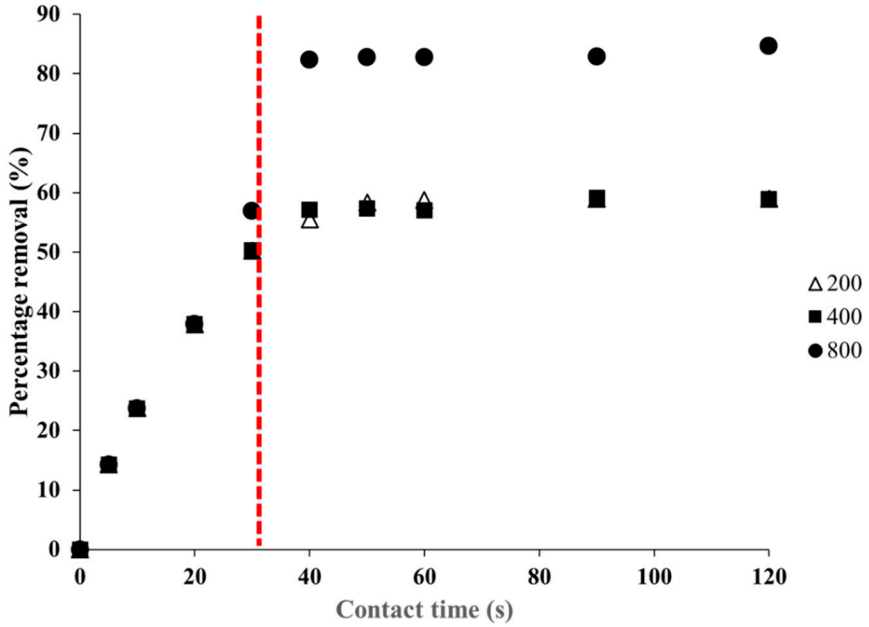

Figure 8. Percentage of diclofenac removal with contact time.

Kinetic analysis was analyzed using three models which were pseudo-first-order (PFO), pseudo-second-order (PSO) and Langmuir–Hinshelwood (LH) kinetic (Figure 8). Since the linearization of nonlinear data disturbs the data's error structure, this makes it harder to assess uncertainty, which is often reported as the 95% confidence interval range [20]. Hence, non-linear regression is preferable for kinetic model fitting since it is conducted on the same abscissa with a linear regression plot, showing more accurate calculations. Figure 9a,b depict the experimental and calculated data plot on pseudo-first and pseudo-second kinetic models, respectively, while Figure 9c shows the Langmuir–Hinshelwood (L-H) model with an unfit data plot. This L-H plot is abundantly being studied in photocatalysis study. However, for the study of batch removal, it has limited applications in heterogeneous catalytic systems since it usually offers negative-order kinetics, which cause erroneous results to be obtained as the kinetic rate parameters estimated at intrinsic kinetic conditions fail to predict the reaction rate when mass transport limitation also plays a role [32]. Another limitation of the Langmuir–Hinshelwood mechanism is that it does not account for the possibility of multiple reaction pathways, which can lead to different reaction products. Additionally, the assumption of random reactions between adsorbed species may not always be accurate, as some surface structures may favor certain reaction pathways over others. Lastly, the Langmuir–Hinshelwood mechanism assumes that the catalyst surface is homogeneous, while real catalysts often have heterogeneous surface structures that can affect the reaction kinetics. A previous recent finding claims that the validity of the L-H model in photocatalytic reaction could be a misinterpretation, and without proper experimental evidence, it is dubious [32,33].

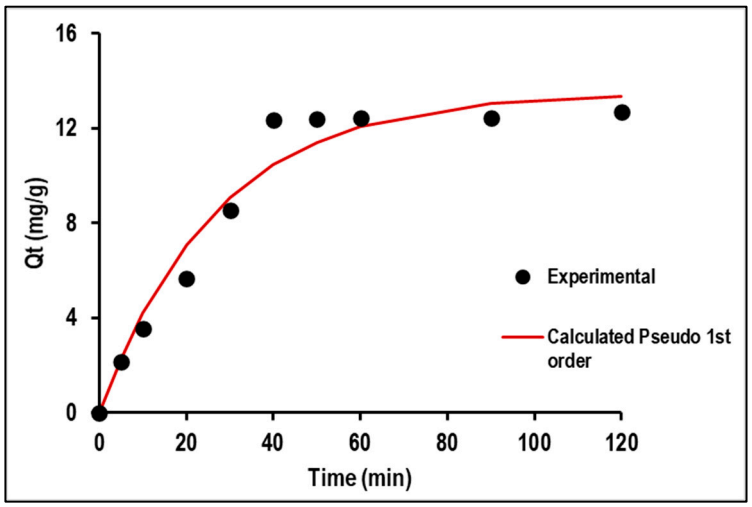

(**a**)

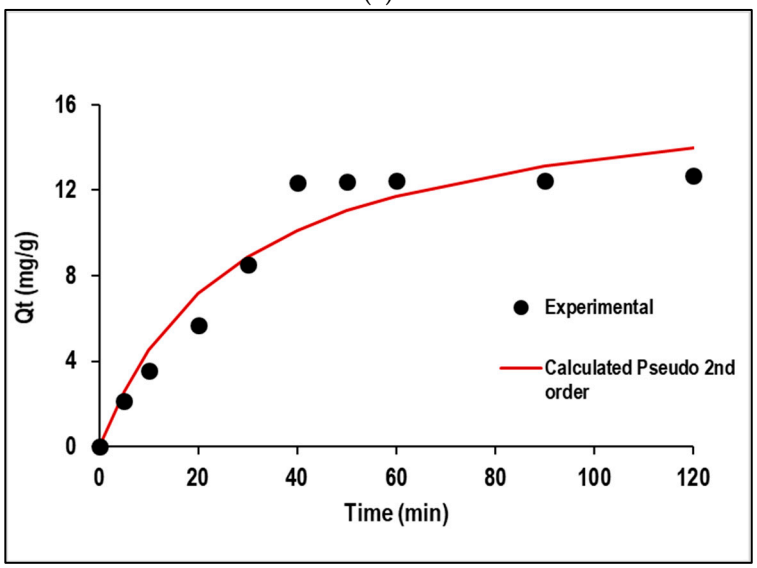

(**b**)

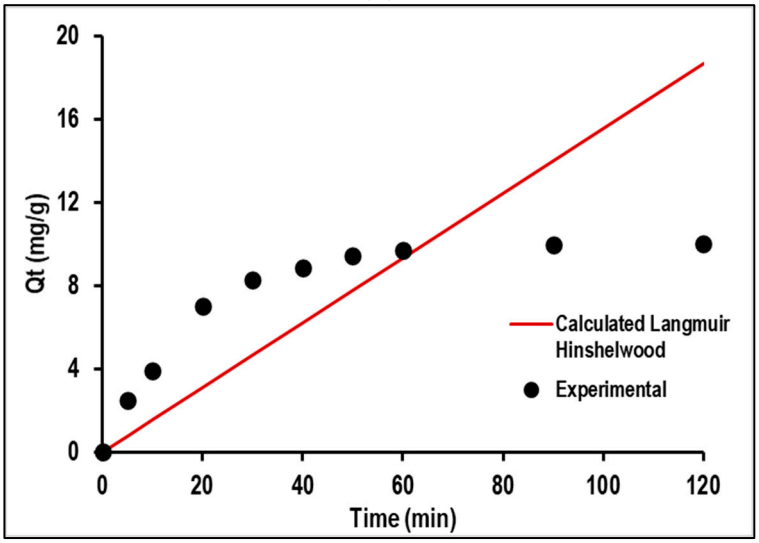

(**c**)

Figure 9. Kinetics of 100 ppm diclofenac removal using photocatalysis reaction (800 µL of TiO_2) as modeled using the pseudo-first-order (**a**), pseudo-second-order (**b**) and Langmuir–Hinshelwood (**c**) models (data at time zero are omitted due to natural logarithm transformation restriction).

Considering the statistical indicators, pseudo-first-order is more accurate in describing the diclofenac removal kinetic profiles than PSO and LH based on error functions analysis with the lowest SSE and AICc, with an R^2 nearest to 1.0 (Table 3). Kinetic analysis using the PSO model at 100 ppm of diclofenac sodium gives a value of equilibrium adsorption capacity, with a q_e of 13.52 mg g^{-1} (Table 4). It was inferred that the three kinetics models discovered to be suitable for fitting the current adsorption kinetics data are as follows: pseudo-first-order > pseudo-second-order > Langmuir–Hinshelwood. As far as diclofenac removal is concerned, the PFO was the best model for the crosslinked soy polysaccharide-based hydrogel nanostructure [34–36].

Table 3. Statistical analysis for removal of sodium diclofenac using 800 µL TiO_2 loading amount in photocatalytic reaction.

Model	RMSE	R^2	AICc
Pseudo-1st-order	0.526	0.997	0.558
Pseudo-2nd-order	1.271	0.971	5.064
Langmuir-Hinshelwood	3.344	0.631	28.47

Table 4. Model constants for the kinetics study of removal of sodium diclofenac.

Model	Adsorption Capacity, qe (mg/g)	Constant, k (95% Confidence Interval)
Pseudo-1st-order	13.52	0.04 (0.023 to 0.05)
Pseudo-2nd-order	17.23	0.002(0.0065 to 0.004059)
L-H	1.33	0.07(0.0032 to 0.0562)

The pseudo-first-order model was utilized to fit data for all TiO_2 loadings, and the data showed excellent agreement with the pseudo-first-order equation (Figure 10) with all regressed lines showing correlation coefficients, $R^2 > 0.99$. As a result, it is reasonable to conclude that the process is pseudo-first-order rather than pseudo-second-order or Langmuir–Hinshelwood. It is also possible that adsorption happens in nature as physisorption, which portray the physical adsorption between two-phase system bulk that is reversible in nature [37–39]. The present study also shows accordance with the findings of a previous analysis of adsorption using a ZnO-chitosan nanocomposite as the nanocellulose component [40].

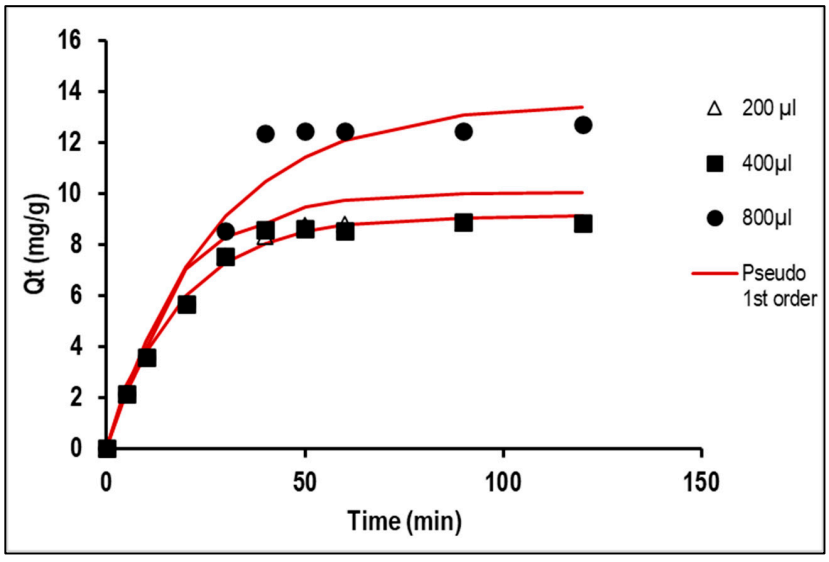

Figure 10. Experimental data versus calculated data (line) on pseudo-first-order kinetic analysis of TiO_2 loading effect on removal of sodium diclofenac sodium under photocatalysis.

4. Conclusions

We developed an adsorbent comprising nanocellulose that was obtained from sago waste. Fe_3O_4/TiO_2 was added to the nanocellulose to give a photocatalytic adsorbent. The system was able to remove diclofenac from industrial wastewater with 57.5% with 200 µL of TiO_2, and this increased up to 82.4% with 800 µL of TiO_2. The maximum removal capacity was found to be 13.3 mg/g. The kinetics was well fitted with the pseudo-first-order model, which gave a qe of 13.52 mg/g. The statistical analyses showed the lowest AICc and RSME values of 0.56 and 0.53, respectively, and the highest correlation coefficient, R^2, of 0.99. This research has demonstrated the synergistic interaction of adsorption and photocatalysis reactions for environmental pollutant removal.

Author Contributions: Conceptualization, N.C.S. and A.A.B.; methodology, D.K. and N.S.H.S.; formal analysis, N.C.S. and A.A.B.; writing—original draft preparation, N.C.S.; writing—review and editing, N.C.S. and A.A.B.; supervision, C.D.W.; funding acquisition, C.D.W. All authors have read and agreed to the published version of the manuscript.

Funding: This research was funded by Yayasan Universiti Teknologi PETRONAS Fundamental Research Grant (YUTP), 015LC0-256.

Institutional Review Board Statement: Not applicable.

Informed Consent Statement: Not applicable.

Data Availability Statement: Data is contained within the article.

Acknowledgments: The authors would like to thank Yayasan Universiti Teknologi PETRONAS Fundamental Research Grant (YUTP), 015LC0-256 for the project funding and the technical support provided by Mohd Yunus Abd Shukor, Biochemistry Department, Faculty of Biotechnology & Biomolecular Sciences, Universiti Putra Malaysia.

Conflicts of Interest: The authors declare no conflict of interest.

References

1. Benotti, M.J.; Trenholm, R.A.; Vanderford, B.J.; Holady, J.C.; Stanford, B.D.; Snyder, S.A. Pharmaceuticals and endocrine disrupting compounds in u.s. drinking water. *Environ. Sci. Technol.* **2009**, *43*, 597–603. [CrossRef] [PubMed]
2. Hanif, H.; Waseem, A.; Kali, S.; Qureshi, N.A.; Majid, M.; Iqbal, M.; Ur-Rehman, T.; Tahir, M.; Yousaf, S.; Iqbal, M.M.; et al. Environmental risk assessment of diclofenac residues in surface waters and wastewater: A hidden global threat to aquatic ecosystem. *Environ. Monit. Assess.* **2020**, *192*, 204. [CrossRef] [PubMed]
3. Steven, T.; Nawaz, R.; Sahrin, N.T.; Lee, K.M.; Bianchi, C.L.; Chong, F.K. H_2O_2-assisted Sonophotocatalytic Degradation of Diclofenac Using a Visible Light-Active Flower-like Micron-Sized TiO_2 Photocatalyst. *Malays. J. Chem.* **2021**, *23*, 108–125. [CrossRef]
4. Abou-Zeid, R.E.; Khiari, R.; El-Wakil, N.; Dufresne, A. Current State and New Trends in the Use of Cellulose Nanomaterials for Wastewater Treatment. *Biomacromolecules* **2018**, *20*, 573–597. [CrossRef]
5. Reshmy, R.; Thomas, D.; Philip, E.; Paul, S.A.; Madhavan, A.; Sindhu, R.; Binod, P.; Pugazhendhi, A.; Sirohi, R.; Tarafdar, A.; et al. Potential of nanocellulose for wastewater treatment. *Chemosphere* **2021**, *281*, 130738. [CrossRef]
6. Addamo, M.; Augugliaro, V.; Di Paola, A.; Garcia-Lopez, E.; Loddo, V.; Marci, G.; Molinari, R.; Palmisano, L.; Schiavello, M. Preparation, Characterization, and Photoactivity of Polycrystalline Nanostructured TiO_2 Catalysts. *J. Phys. Chem. B* **2004**, *108*, 3303–3310. [CrossRef]
7. Zhang, S.; Guo, S.; Li, A.; Liu, D.; Sun, H.; Zhao, F. Low-cost bauxite residue-MoS_2 possessing adsorption and photocatalysis ability for removing organic pollutants in wastewater. *Sep. Purif. Technol.* **2022**, *283*, 120144. [CrossRef]
8. Pan, Y.; Zhang, Y.; Huang, Y.; Jia, Y.; Chen, L. Enhanced photocatalytic oxidation degradability for real cyanide wastewater by designing photocatalyst GO/TiO_2/ZSM-5: Performance and mechanism research. *Chem. Eng. J.* **2022**, *428*, 131257. [CrossRef]
9. Leong, S.; Razmjou, A.; Wang, K.; Hapgood, K.; Zhang, X.; Wang, H. TiO_2 based photocatalytic membranes: A review. *J. Membr. Sci.* **2014**, *472*, 167–184. [CrossRef]
10. Kanakaraju, D.; Motti, C.A.; Glass, B.D.; Oelgemoller, M. Photolysis and TiO_2-catalysed degradation of diclofenac in surface and drinking water using circulating batch photoreactors. *Environ. Chem.* **2014**, *11*, 51–62. [CrossRef]
11. Mu, R.; Xu, Z.; Li, L.; Shao, Y.; Wan, H.; Zheng, S. On the photocatalytic properties of elongated TiO_2 nanoparticles for phenol degradation and Cr(VI) reduction. *J. Hazard. Mater.* **2010**, *176*, 495–502. [CrossRef] [PubMed]

12. Chong, M.N.; Jin, B.; Chow, C.W.K.; Saint, C. Recent developments in photocatalytic water treatment technology: A review. *Water Res.* **2010**, *44*, 2997–3027. [CrossRef]
13. Villa, S.; Caratto, V.; Locardi, F.; Alberti, S.; Sturini, M.; Speltini, A.; Maraschi, F.; Canepa, F.; Ferretti, M. Enhancement of TiO_2 NPs Activity by Fe_3O_4 Nano-Seeds for Removal of Organic Pollutants in Water. *Materials* **2016**, *9*, 771. [CrossRef]
14. Zaidi, N.A.H.M.; Lim, L.B.L.; Usman, A.; Kooh, M.R.R. Efficient adsorption of malachite green dye using *Artocarpus odoratissimus* leaves with artificial neural network modelling. *Desalin. Water Treat.* **2018**, *101*, 313–324. [CrossRef]
15. Rahimi Kooh, M.R.; Thotagamuge, R.; Chau, Y.-F.C.; Mahadi, A.H.; Lim, C.M. Machine learning approaches to predict adsorption capacity of *Azolla pinnata* in the removal of methylene blue. *J. Taiwan Inst. Chem. Eng.* **2022**, *132*, 104134. [CrossRef]
16. Kanakaraju, D.; Lim, Y.-C.; Pace, A. Magnetic hybrid TiO_2/Alg/FeNPs triads for the efficient removal of methylene blue from water. *Sustain. Chem. Pharm.* **2018**, *8*, 50–62. [CrossRef]
17. Hami, H.K.; Ruba, F.A.; Amel, S.M.; Asma, A.M. An overview of using error function in adsorption isotherm modeling. *Muthanna J. Pure Sci. (MJPS)* **2021**, *8*, 22–30. [CrossRef]
18. Naduparambath, S.; Purushothaman, E. Sago seed shell: Determination of the composition and isolation of microcrystalline cellulose (MCC). *Cellulose* **2016**, *23*, 1803–1812. [CrossRef]
19. Aghamali, A.; Khosravi, M.; Hamishehkar, H.; Modirshahla, N.; Behnajady, M.A. Preparation of novel high performance recoverable and natural sunlight-driven nanocomposite photocatalyst of Fe_3O_4/C/TiO_2/N-CQDs. *Mater. Sci. Semicond. Process.* **2018**, *87*, 142–154. [CrossRef]
20. Martínez, C.; Canle, L.M.; Fernández, M.I.; Santaballa, J.A.; Faria, J. Aqueous degradation of diclofenac by heterogeneous photocatalysis using nanostructured materials. *Appl. Catal. B Environ.* **2011**, *107*, 110–118. [CrossRef]
21. Subramanyam, B.; Das, A. Linearised and non-linearised isotherm models optimization analysis by error functions and statistical means. *J. Environ. Health Sci. Eng.* **2014**, *12*, 92. [CrossRef] [PubMed]
22. Azizian, S. Kinetic models of sorption: A theoretical analysis. *J. Colloid Interface Sci.* **2004**, *276*, 47–52. [CrossRef]
23. Basirun, A.A.; Khudri, M.A.M.R.S.; Yasid, N.A.; Othman, A.R.; Johari, W.L.W.; Shukor, M.Y.; Halmi, M.I.E. Kinetic Analysis for the Removal of Copper Using *Durvillaea antarctica*. *J. Environ. Microbiol. Toxicol.* **2019**, *7*, 32–35. [CrossRef]
24. Kumar, M.; Tamilarasan, R. Kinetics, equilibrium data and modeling studies for the sorption of chromium by *Prosopis juliflora* bark carbon. *Arab. J. Chem.* **2017**, *10*, S1567–S1577. [CrossRef]
25. Segal, L.; Creely, J.J.; Martin, A.E., Jr.; Conrad, C.M. An Empirical Method for Estimating the Degree of Crystallinity of Native Cellulose Using the X-Ray Diffractometer. *Text. Res. J.* **1959**, *29*, 786–794. [CrossRef]
26. Zheng, J.; Wu, Y.; Zhang, Q.; Li, Y.; Wang, C.; Zhou, Y. Direct liquid phase deposition fabrication of waxberry-like magnetic Fe_3O_4@TiO_2 core-shell microspheres. *Mater. Chem. Phys.* **2016**, *181*, 391–396. [CrossRef]
27. Shi, F.; Li, Y.; Zhang, Q.; Wang, H. Synthesis of Fe_3O_4/C/TiO_2 magnetic photocatalyst via vapor phase hydrolysis. *Int. J. Photoenergy* **2012**, *2012*, 365401. [CrossRef]
28. Salamat, S.; Younesi, H.; Bahramifar, N. Synthesis of magnetic core–shell Fe_3O_4@TiO_2 nanoparticles from electric arc furnace dust for photocatalytic degradation of steel mill wastewater. *RSC Adv.* **2017**, *7*, 19391–19405. [CrossRef]
29. Gopalakannan, V.; Viswanathan, N. One pot synthesis of metal ion anchored alginate–gelatin binary biocomposite for efficient Cr(VI) removal. *Int. J. Biol. Macromol.* **2016**, *83*, 450–459. [CrossRef]
30. Ben Hammouda, S.; Adhoum, N.; Monser, L. Synthesis of magnetic alginate beads based on Fe_3O_4 nanoparticles for the removal of 3-methylindole from aqueous solution using Fenton process. *J. Hazard. Mater.* **2015**, *294*, 128–136. [CrossRef]
31. Wei, J.; Yang, Z.; Sun, Y.; Wang, C.; Fan, J.; Kang, G.; Zhang, R.; Dong, X.; Li, Y. Nanocellulose-based magnetic hybrid aerogel for adsorption of heavy metal ions from water. *J. Mater. Sci.* **2019**, *54*, 6709–6718. [CrossRef]
32. Gangwal, V.; Van Der Schaaf, J.; Kuster, B.; Schouten, J. The effect of mass transport limitation on the estimation of intrinsic kinetic parameters for negative order reactions. *Appl. Catal. A Gen.* **2004**, *274*, 275–283. [CrossRef]
33. Lazar, M.A.; Varghese, S.; Nair, S.S. Photocatalytic Water Treatment by Titanium Dioxide: Recent Updates. *Catalysts* **2012**, *2*, 572–601. [CrossRef]
34. Anirudhan, T.; Rejeena, S. Photocatalytic degradation of eosin yellow using poly (pyrrole-co-aniline)-coated TiO_2/nanocellulose composite under solar light irradiation. *J. Mater.* **2015**, *2015*, 636409. [CrossRef]
35. Rathod, M.; Moradeeya, P.G.; Haldar, S.; Basha, S. Nanocellulose/TiO_2 composites: Preparation, characterization and application in the photocatalytic degradation of a potential endocrine disruptor, mefenamic acid, in aqueous media. *Photochem. Photobiol. Sci.* **2018**, *17*, 1301–1309. [CrossRef]
36. Yue, Y.; Shen, S.; Cheng, W.; Han, G.; Wu, Q.; Jiang, J. Construction of mechanically robust and recyclable photocatalytic hydrogel based on nanocellulose-supported CdS/MoS_2/Montmorillonite hybrid for antibiotic degradation. *Colloids Surf. A Physicochem. Eng. Aspects* **2022**, *636*, 128035. [CrossRef]
37. Kumar, K.V.; Porkodi, K.; Rocha, F. Langmuir–Hinshelwood kinetics—A theoretical study. *Catal. Commun.* **2008**, *9*, 82–84. [CrossRef]
38. Tran, H.N.; You, S.; Hosseini-Bandegharaei, A.; Chao, H. Mistakes and inconsistencies regarding adsorption of contaminants from aqueous solutions: A critical review. *Water Res.* **2017**, *120*, 88–116. [CrossRef]

39. Kopinke, F.-D.; Georgi, A.; Goss, K.-U. Comment on "Mistakes and inconsistencies regarding adsorption of contaminants from aqueous solution: A critical review, published by Tran et al. [Water Research 120, 2017, 88–116]". *Water Res.* **2018**, *129*, 520–521. [CrossRef]
40. Zango, Z.U.; Dennis, J.O.; Aljameel, A.I.; Usman, F.; Mohammed Ali, M.K.; Abdulkadir, B.A.; Algessair, S.; Aldaghri, O.A.; Ibnaouf, K.H. Effective removal of methylene blue from simulated wastewater using ZnO-chitosan nanocomposites: Optimization, kinetics, and Isotherm studies. *Molecules* **2022**, *27*, 4746. [CrossRef]